Bulletin of the New Zealand Society for Earthquake Engineering, Vol. 50, No. 2, June 2017

STRONG GROUND MOTION OBSERVATIONS OF ENGINEERING INTEREST FROM THE 14 NOVEMBER 2016 M_W7.8 KAIKŌURA, NEW ZEALAND EARTHQUAKE

Brendon A. Bradley[1,2], Hoby N.T. Razafindrakoto[3] and M. Ahsan Nazer[3]

(Submitted *March 2017*; Reviewed *April 2017*; Accepted *May 2017*)

ABSTRACT

This paper provides a brief discussion of observed strong ground motions from the 14 November 2016 M_w7.8 Kaikōura earthquake. Specific attention is given to examining observations in the near-source region where several ground motions exceeding 1.0g horizontal are recorded, as well as up to 2.7g in the vertical direction at one location. Ground motion response spectra in the near-source, North Canterbury, Marlborough and Wellington regions are also examined and compared with design levels. Observed spectral amplitudes are also compared with predictions from empirical and physics-based ground motion modelling.

INTRODUCTION

On 14 November 2016 at 12:02 AM local time, the M_w7.8 'Kaikōura' earthquake occurred along the east coast of the upper South Island, New Zealand [1, 2]. The earthquake initiated in the Waiau Plains in North Canterbury, and involved multiple fault segments as the rupture generally propagated northward over 150km to Cape Campbell in Marlborough. It was the largest recorded earthquake in New Zealand since the 1855 $M_w8.2-8.3$ Wairarapa earthquake [3].

Given the geographical proximity of the source in a largely rural region of New Zealand, the impacts in the near-source region were largely geological and geotechnical in nature, namely surface rupture [4], landslides [5], and localized ground failure, resulting in damage to coastal transportation infrastructure [6] and the formation of landslide dams.

This paper is intended to provide insights into the observed ground motion records from the Kaikōura earthquake in order to understand the earthquake-induced demands imposed on the natural and built environment. In the subsequent sections we first summarize the tectonic setting and inferred rupture, followed by a discussion of the observed ground motions in various contexts, and then finally inferences based on ground motion modelling.

TECTONIC SETTING AND INFERRED CAUSATIVE RUPTURE

Observations and multiple geophysical and geodetic methods highlight the source complexity of this earthquake with numerous fault segments rupturing [4, 7].

Figure 1 illustrates the rupture segment geometries of the causative faults presented by Bradley et al. [9], and adopted here for ground motion observation and modelling interpretations. For reference, the surface trace of fault segments that are considered in the InSAR+GPS inversion of Hamling et al. [8], significant aftershocks, and mapped active faults are also shown.

Litchfield et al. [4] have so far identified at least nine fault segments (The Humps, Hundelee, Conway-Charwell, Upper Kowai, Fidget, Jordan Thrust, Papatea, Kekerengu, and Needles Faults) that have evidence of surface fault rupture. Eight of these faults are located onshore with displacements obtained principally from direct field measurement of identifiable features; while rupture of the Needless Fault, located offshore at the northern end of the ruptured faults, has been identified from seabed uplift [10]. Most notably, essentially no surface rupture of the Hope Fault (the major fault identified *apriori* in the region [11]) has been mapped to date [4].

GROUND MOTION OBSERVATIONS

A Regional View

A total of 224 Volume 1 ground motion records were obtained from GeoNet, and processed to obtain realistic spectral ordinates over the vibration period range of T=0.01-10s, as discussed in [9]. Figure 2 illustrates the three component velocity time series of the GeoNet ground motion station recordings and their location relative to the causative rupture, which have a range in source-to-site distances of R_{rup}=0-216 km. As would be expected, the highest velocities are evident in the near-source region. However, the nature of the waveforms vary significantly at similar R_{rup} values depending on the back-azimuth from the site to the rupture - those stations in proximity to the southern end of the rupture in North Canterbury (e.g. stations WTMC, WIGC, HSES) exhibit high-amplitude short-duration ground motions, while those at the north end of the rupture in northern Marlborough (e.g. SEDS, BWRS) and Wellington (e.g. FKPS, NEWS) have substantially longer duration and also well-defined multiple wave packets indicating 'delayed' rupture initiation of several segments. Central South Island stations, such as in Molesworth (MOLS) and Wairau Valley (WVFS), also exhibit two clear velocity wave packets.

In total, 47, 16, and 5 ground motions were observed with peak ground acceleration, $PGA > 0.1$g, 0.2g, and 0.5g, respectively, and will contribute substantially to the existing database of NZ strong motion records [e.g. 12].

[1] *Corresponding Author. Professor, Department of Civil and Natural Resources Engineering, University of Canterbury, New Zealand, brendon.bradley@canterbury.ac.nz*
[2] *UPS Visiting Professor, Stanford University, CA*
[3] *Postdoctoral fellow, Department of Civil and Natural Resources Engineering, University of Canterbury, New Zealand*

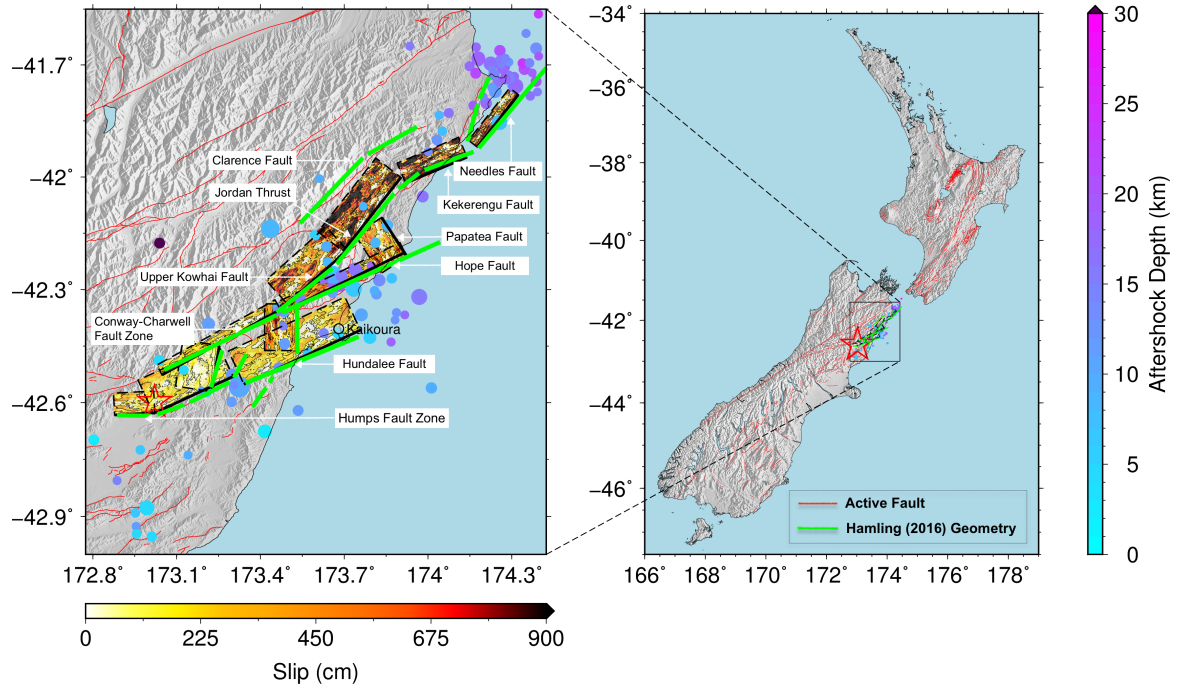

Figure 1: Location of the M_w7.8 Kaikōura earthquake and causative faults on the east coast of the South Island, New Zealand. Hypocentre is marked with a red star. Surface trace of the source inversion of [8] shown in green, and adopted kinematic rupture model faults shown as planes coloured by slip amplitude and contoured by rupture time. $M_w > 4.5$ GeoNet CMT aftershocks till 15 Dec 2016 also illustrated as a function of centroid depth. Figure after [9].

The subsequent sections discuss specific aspects of observed ground motions in regions of particular interest.

Accelerations in the Near-Fault Region

Figure 3 illustrates four strong motion stations that are located in the immediate region of the causative faults. Station WTMC is located immediately near the inferred epicenter in Waiau; KIKS in Kaikōura, approximately halfway along the north-south extent of the rupturing faults; and KEKS and WDFS are located in Kekerengu and Ward, respectively, at the northern end of the rupturing faults.

Because of its location near the epicenter (see Figure 1), the ground motion observed at WTMC (Figure 3a) indicates a short strong motion duration relative to the other three near-fault stations. The ground motion accelerations at WTMC exceed 1.0g in both horizontal directions, and notably the acceleration in the vertical direction reaches 2.7g (with a 100Hz high-cut filter). It is worth noting that the vertical accelerations exhibit strong asymmetry toward higher amplitudes in the positive direction (e.g. two exceedances of +2.0g, while negative accelerations are limited to a little over -1.0g). This phenomena has been documented in several ground motions from past earthquakes such as the 2011 Christchurch, New Zealand [13, 14], and the 2008 Iwate-Miyagi, Japan [15–17] earthquakes. As demonstrated by others [17, 18], such asymmetry results from the varying near surface soil shear strength during induced compression and dilation. Furthermore, independent evidence of the extreme vertical accelerations in the vicinity of the WTMC site were seen (by the first author and others during field reconnaissance) in the form of bearing pads significantly moving (and, in one case, coming out from) between bridge abutment and girders at two bridges on Inland Road (SH70), within 2km from the WTMC station.

The KIKS station recorded relatively small levels of ground motion acceleration, given its location on a peninsula near the north-south mid-point of the rupturing fault segments, with horizontal and vertical peak accelerations of approximately 0.22g and 0.27g, respectively. The horizontal peak velocities are also a similarly small PGV=41-45cm/s, as compared to the other three stations in Figure 3 which generally have PGV >80cm/s (velocity time series at all four stations are shown in Figure 2).

Figure 3c and 3d illustrate the recorded ground motion accelerations at Kekerengu (KEKS) and Ward (WDFS) stations, which are located near the northern end of the rupturing faults, and are themselves located 16km apart. Both of these stations clearly illustrate acceleration records which are dominated by two predominant wave packets, one near $t = 60s$, and the other near $t = 80s$. Because of the fact that the KEKS station is within 2.5km of the mapped surface rupture of the Kekerengu fault [4] (with surface rupture displacements of 5-10m horizontal, and 1-2m vertical in the vicinity) it is reasonable to assume that the peak accelerations in the KEKS record correspond to the through-going rupture past this location. In contrast to KEKS, at the WDFS station the peak accelerations occur near $t = 80s$, which based on the source model in Figure 1 is inferred as the result of rupture of the Needles fault. [8] inferred some (small) slip on the Grassmere fault located onshore from the Needles fault (and thus closer to the WDFS station). Further inferences of the source rupture from these observed ground motions are discussed in [9].

Observed Response Spectra

Figure 4 illustrates the observed response spectra of stations in the near-fault region (i.e. Figure 3) as well as those in selected regions of North Canterbury, Marlborough, and Wellington. For reference, the site class C and D response spectra from NZS1170.5:2004 [19] for Z=0.4 and a 500 year return period are also shown (it is acknowledged that the value of Z varies over the sites/regions illustrated, but a common value is depicted for consistent reference). Nominal site classes for each station can be found in Kaiser et al. [20]. At short vibration periods ($T < 1s$) it can be seen that the largest response spectral am-

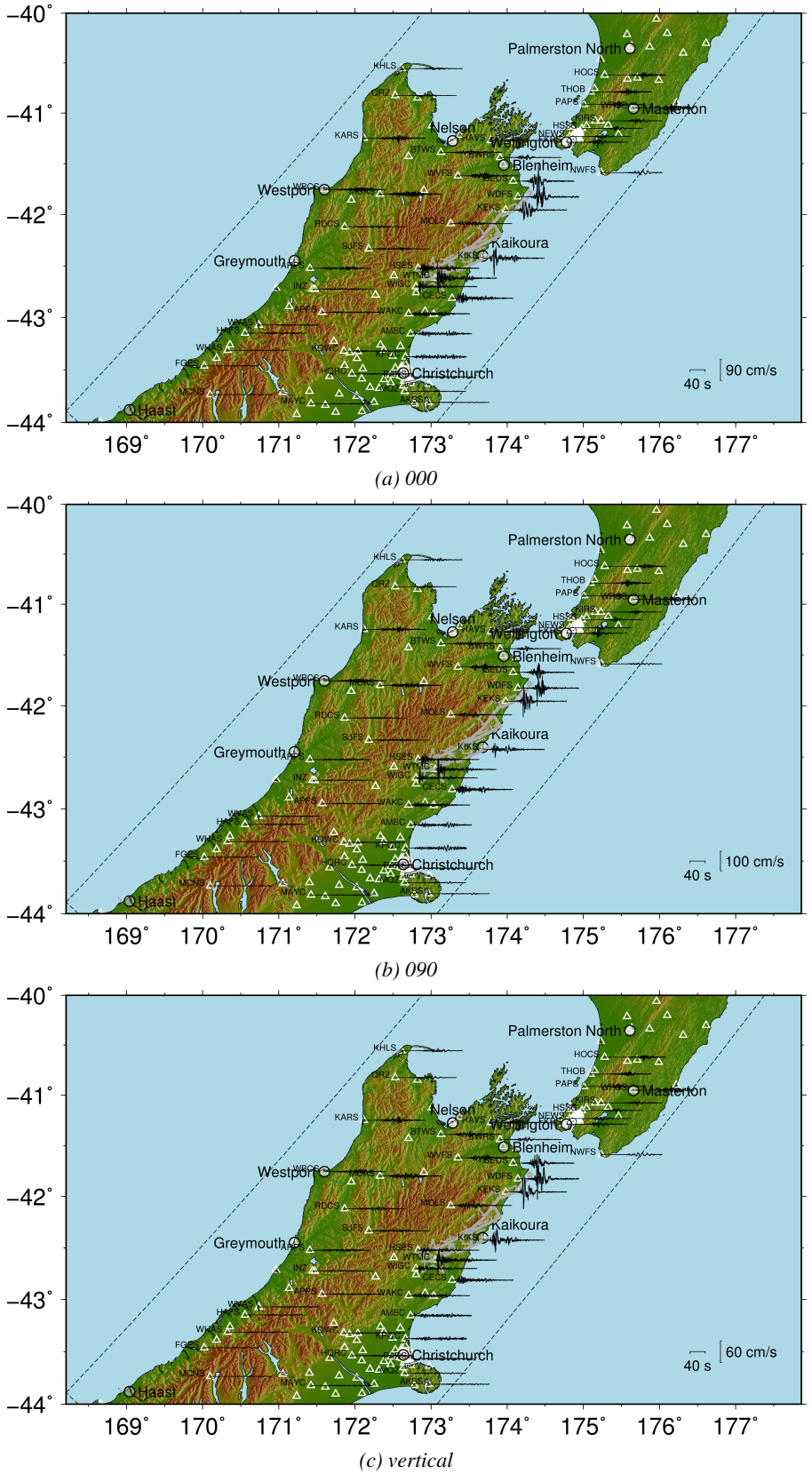

(a) 000

(b) 090

(c) vertical

Figure 2: Spatial illustration of the variation in observed ground motion velocities at selected strong motion stations for: (a) north-south (000); (b) east-west (090); and (c) vertical components.

plitudes are observed in the near-fault region (Figure 4a) at the WTMC, KEKS, and WDFS stations, but also that large amplitudes are seen at the WIGC (Waiau Gorge) station in North Canterbury (Figure 4b) and SEDS (Seddon) station in Marlborough (Figure 4c). The short period ground motion amplitudes in Kaikōura and Wellington, other locations in North Cantebrury and Marlborough, have appreciably smaller values as a result of the attenuation associated with larger source-to-site distances.

The shape of the response spectra in Wellington (Figure 4d) are appreciably different than those in the other regions, principally in relation to their predominance of long-period ground motion

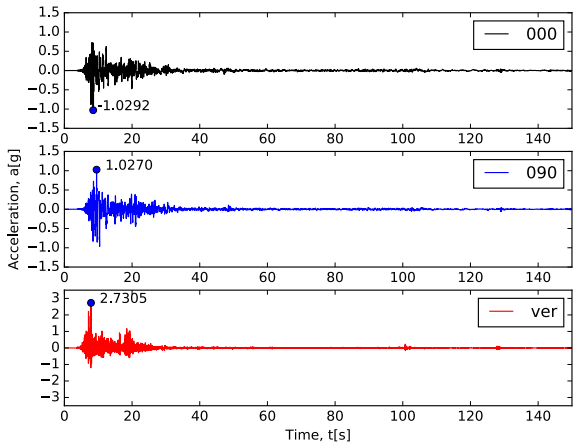

(a) Waiau, WTMC

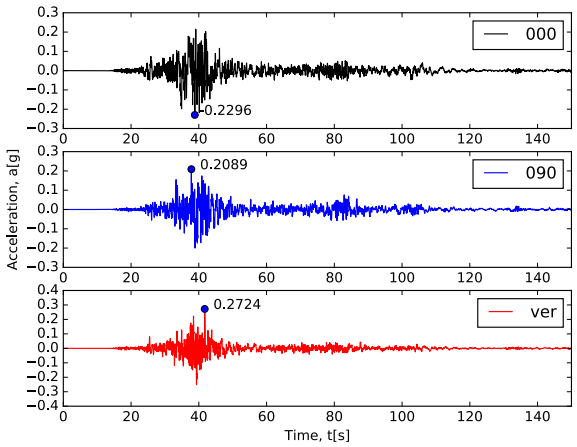

(b) Kaikōura, KIKS

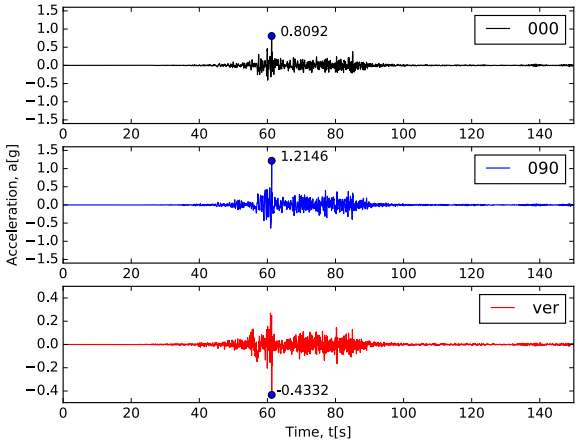

(c) Kekerengu, KEKS

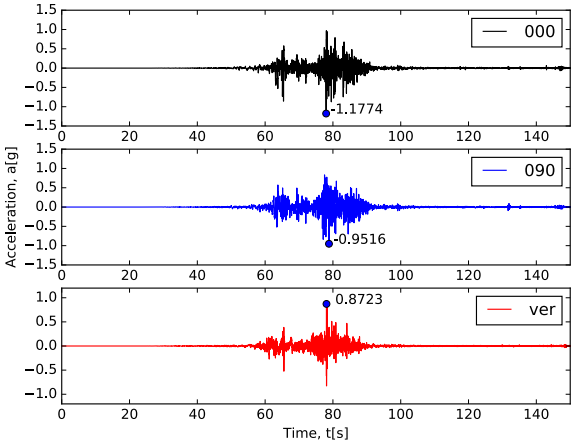

(d) Ward, WDFS

Figure 3: Recorded ground motion accelerations in the immediate vicinity of the rupturing faults (locations noted in Figure 2). 000, 090, and ver represent north-south, east-west and vertical components, respectively. Maximum accelerations in each component are explicitly noted. Different vertical axis scales are used for each station, and between horizontal and vertical components for clarity. Figure after [9].

- the result of both the source-to-site distance (leading to small short period amplitudes, as noted above), but also basin and site response effects [9, 21].

COMPARISON OF OBSERVATIONS WITH GROUND MOTION MODELLING

Bradley et al. [9] provide further insights into the observed ground motions discussed in the previous section via comparison with empirical and physics-based ground motion modelling. Figure 5 illustrates snapshots of the simulated ground motion wavefield (in the form of ground motion velocity at the surface) for nine time instants during the simulation (A video is available at: URL: https://youtu.be/ZbI7rgnZ2U8) [1] During the first 30 seconds of the simulation it can be that the 'southern' fault segments (The Humps, Hundalee, Hope) rupture in a northerly direction. Approximately at $t = 40s$ the delayed rupture initiation at the southern end of the Jordan Thrust starts, and these 'northern' faults (Jordan, Kekerengu, Papatea, Needles) rupture over the following 40 seconds. Finally, after the rupture itself ceases at approximately $t = 80s$, the wavefield, with pronounced directivity migrating to the north east, approaches the lower North Island.

Figure 6 provides a summary of the ground motion intensities over the simulation domain in the form of the peak ground velocity, *PGV* (three-component maximum), and the Modified Mercalli Intensity (MMI) values, based on the MMI-to-PGV correlation of [24]. As implied by the wavefield snapshots in Figure 5, it can be seen that significant directivity occurs to the north east as a result of the fault geometries and rupture sequence (fortunately a significant potion of the $MMI > 8$ region occurs offshore, or in low-population density areas). As a result, the ground motion amplitudes to the south and west of the causative faults were modest in comparison. It can be seen that the Marlborough and Lower North Island was subject to approximately $MMI = 7$ ground motion amplitudes with $PGV = 20 - 40 cm/s$.

Comparison of Response Spectra Modelling and Observations

Figure 7 illustrates the observed and modelled ground motion spectral amplitudes for four vibration periods ($T = 0.0, 0.2, 3.0,$ and $10.0s$) as a function of source-to-site distance. The observed and simulated ground motion amplitudes for the 162 stations

[1] The waveform anomaly near Lon:174.5° Lat:-43.2° is the result of a discontinuity between the domain-wide model [22], with the offshore portion of the Canterbury Velocity model [23]. It is present only in the offshore region and the resulting localized spurious wavefield does not have a material effect on the simulated motion onshore

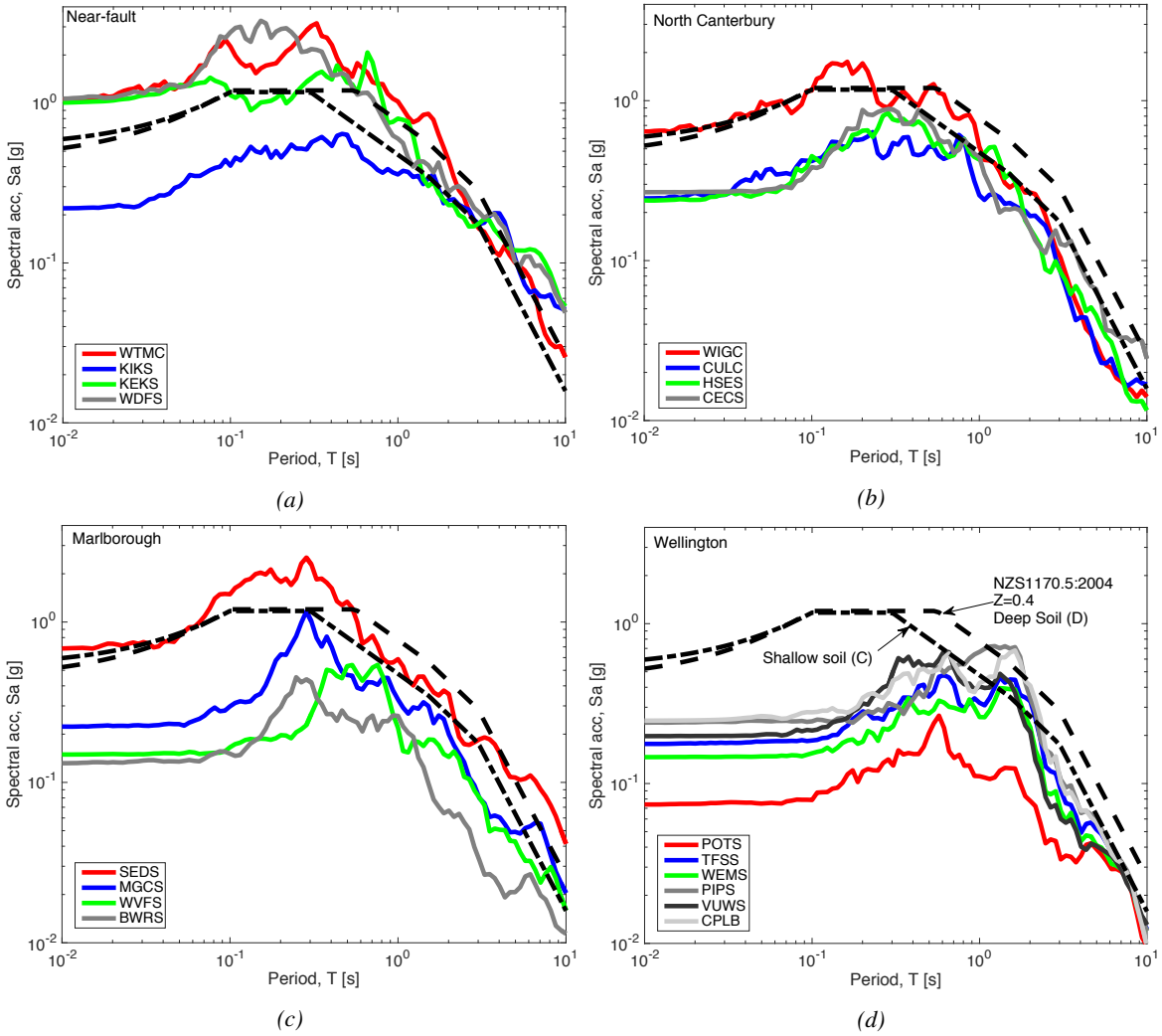

Figure 4: A regional depiction of the geometric mean horizontal response spectra observed in: (a) the near-fault; (b) North Canterbury; (c) Marlborough; and (d) Wellington region. NZS1170.5 design spectra for Z=0.4 and 500 year return period are provided for reference. Four letter station codes in the figure legends can be located spatially in Figure 2.

within the simulation domain are shown. The stations are also separately annotated based on their location in either the North or South Island. In addition to the simulation predictions, for reference, the NZ-specific empirical ground motion model of Bradley et al. [25] is also shown for reference site conditions of $V_{s30} = 250m/s$. It can be seen that the simulation provides a generally good comparison with the observed amplitudes. In particular, the distance attenuation in the observations at short periods (i.e. $T = 0.0$ and $0.2s$) is consistently predicted by the simulations, while the empirical model predicts a slower attenuation; conversely at long periods, the empirical model predicts a faster attenuation than exhibited by both the observed and simulated amplitudes. Although, not easily evident because of the large number of data points present, the simulations and observations are also broadly consistent in the higher-than-average amplitudes of North Island ground motions relative to those in the South Island for the same source-to-site distance - partially attributed to the aforementioned effect of rupture directivity, among other possible effects. Bradley et al. [9] present further details on the predictive capabilities of the empirical and simulation-based methods.

Comparison of Modelled and Observed Significant Duration

In addition to amplitude and frequency content, as conveyed via response spectral ordinates discussed above, strong motion duration is also important for inelastic seismic response. Figure 8 illustrates the observed and modelled 5-95% Significant Duration (D_{s595}) as a function of source-to-site distance. The empirical model is that provided by Afshari and Stewart [26]. It can be seen that the observed ground motions are broadly consistent with the empirical model, however there is a clear distinction between those observations to the north or south of the causative faults (which have lower- and higher-than-average durations). These observations, which are principally the result of the rupture propagation from south to north, are well captured in the simulated ground motion durations. It is also important to note that, as a result of the forward directivity, locations north of the causative faults (e.g. Wellington) have lower than median D_{s595} values for this particular earthquake, which is also discussed in Bradley et al [2017, this issue].

DISCUSSION AND CONCLUSIONS

This paper has provided a summary of observed ground motions from the 14 November 2016 M_w7.8 Kaikōura earthquake. Ground motions were observed at over 200 strong motion sta-

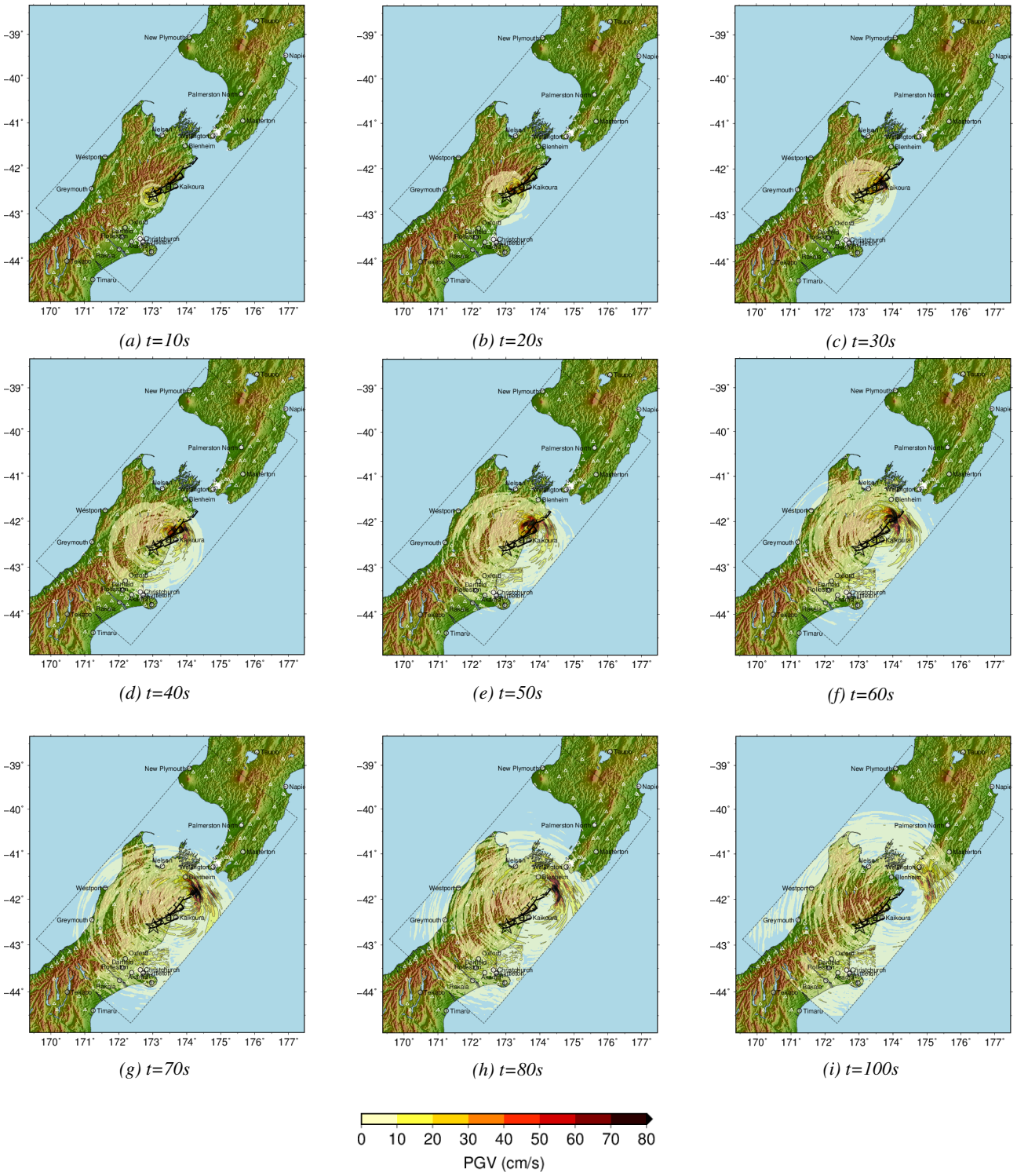

Figure 5: Time snapshots of simulated ground velocity (three component maximum). The causative fault segments and simulation domain are also indicated. A video of the simulation is available in the electronic supplement to this article and at: URL: https://youtu.be/ZbI7rgnZ2U8. Figure after [9].

tions, with 47 ground motions exceeding 0.1g *PGA* - thus providing a significant complement to prior NZ strong motion data. The near-source ground motions clearly highlight the complexity of the earthquake rupture, with multiple wave packets in time clearly evident, and several very large horizontal and vertical amplitudes recorded. The response spectra of observed ground motions illustrated regions with large short and long period ground motion amplitudes. The long period amplitudes in Wellington are of particular note as discussed further in [21].

Despite the rupture complexity of this event, the observed ground motions are broadly consistent with ground motion modelling. Short period ground motion amplitudes are well approximated by empirical and simulation models, although the observations (and simulation modelling) indicate greater attenuation at larger distances ($R_{rup} > 60km$) than in empirical modelling. Long period ground motion amplitudes are, on average, well approximated by the simulation-based modelling, and exceed empirical models at long vibration periods. A strong directivity is seen in the long period spectral amplitudes, which larger values at sites located in the general northward direction from the causative faults. Such

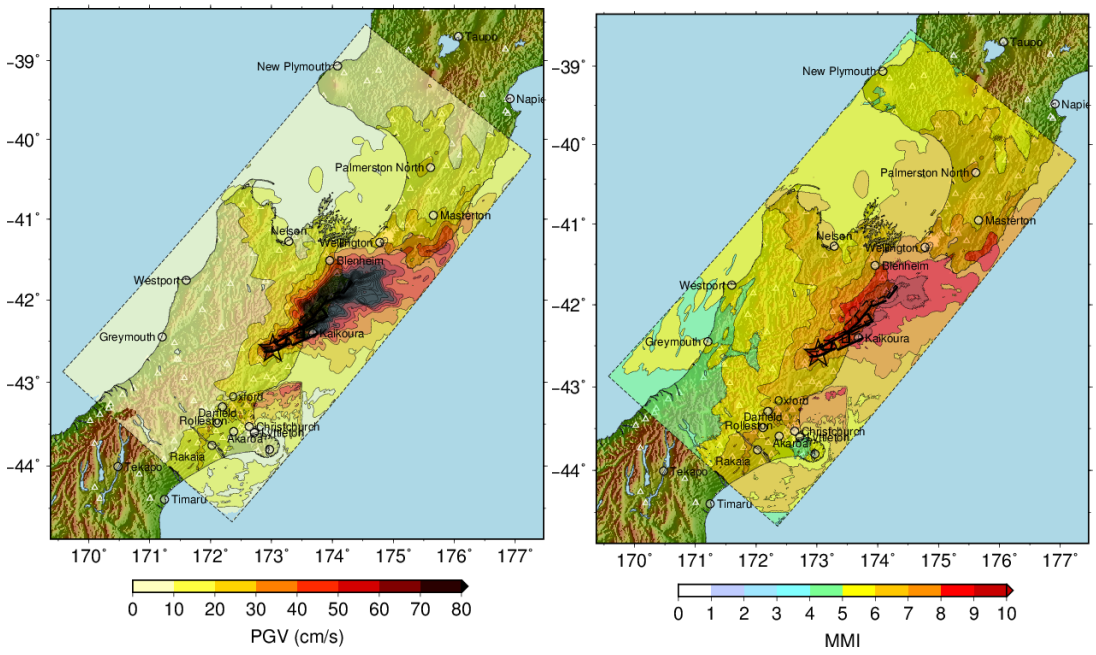

Figure 6: Spatial variation of: (a) peak ground velocity (PGV); and (b) Modified Mercalli Intensity (MMI) from the ground motion simulation (vector maximum of the two horizontal components).

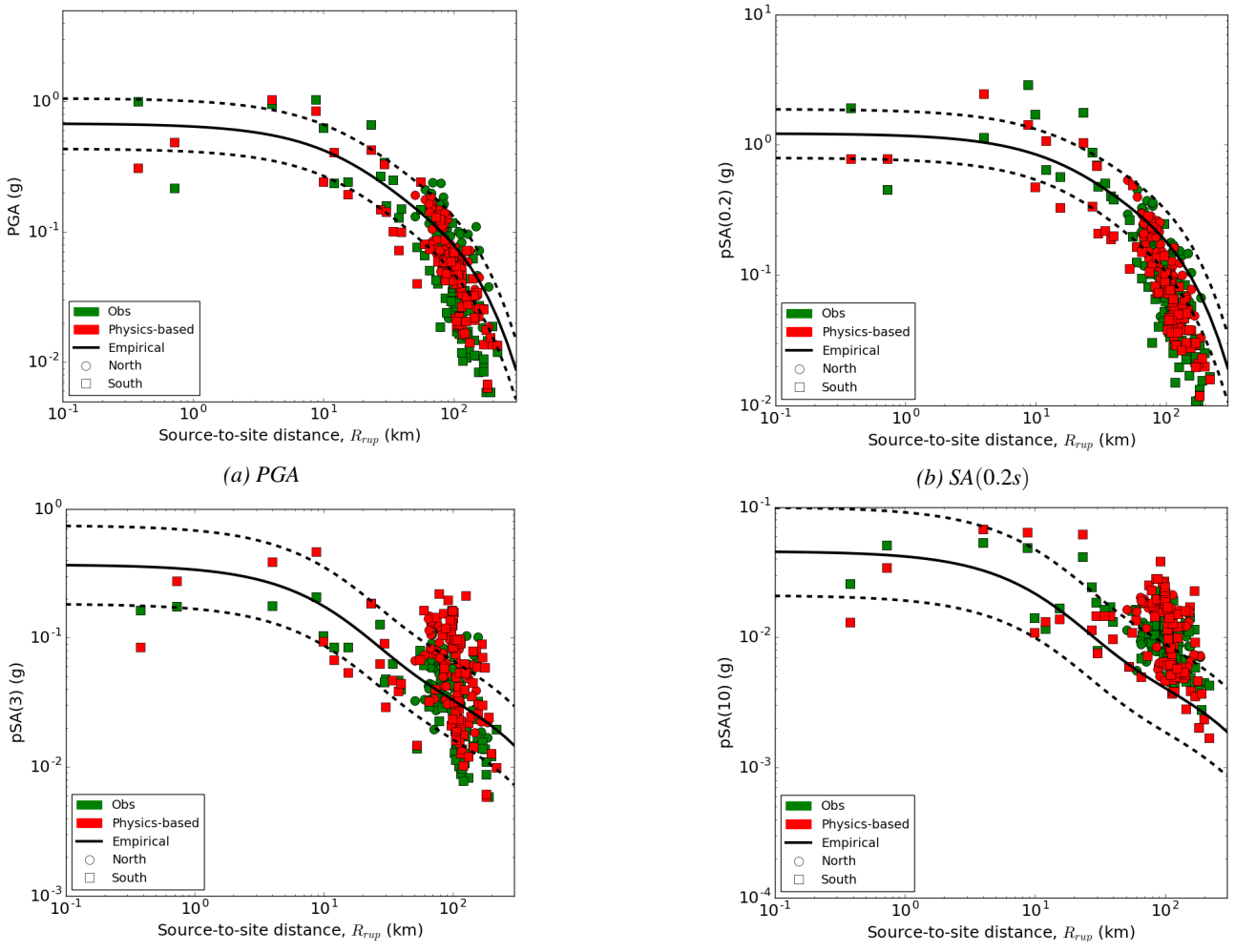

(a) PGA *(b) $SA(0.2s)$*

(c) $SA(3.0s)$ *(d) $SA(10.0s)$*

Figure 7: Observed, simulated, and empirically-predicted geometric mean ground motion intensities as a function of source-to-site distance, R_{rup}. Symbol shape indicates location of the station in the North or South Island. The median, and 16^{th}/84^{th} percentiles of the empirical prediction [25] are represented by solid and dashed lines, respectively (based on a reference $V_{s30} = 250m/s$ condition). Figure after [9].

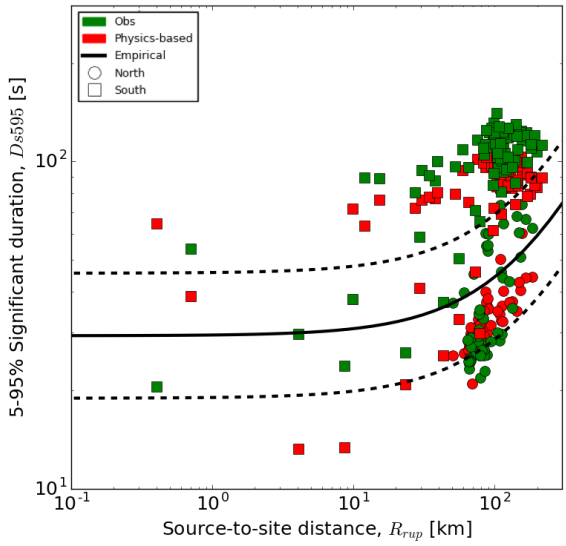

Figure 8: Observed, simulated, and empirically-predicted 5-95% Significant Duration (D_{s595}) as a function of source-to-site distance, R_{rup}. Symbol shape indicates location of the station in the North or South Island. The median, and 16^{th}/84^{th} percentiles of the empirical prediction [26] are represented by solid and dashed lines, respectively (based on a reference $V_{s30} = 250m/s$ condition).

directivity is captured to some extent in the simulations, but not accounted for in the empirical modelling.

ACKNOWLEDGEMENTS

Observed ground motions were obtained from GeoNet (URL: www.geonet.org.nz). This work was also supported by a Royal Society New Zealand Rutherford Discovery Fellowship and QuakeCoRE: The Centre for Earthquake Resilience. This is QuakeCoRE publication number 0147.

REFERENCES

1 USGS (2016). "https://www.usgs.gov/news/magnitude-78-earthquake-new-zealand". URL: https://www.usgs.gov/news/magnitude-78-earthquake-new-zealand.

2 GeoNet (2016). "http://www.geonet.org.nz/quakes/2016p858000".

3 GeoNet (2016). "M 8.2 - 8.3, Wairarapa, 23 January 1855: http://info.geonet.org.nz/display/quake/M+8.2+-+8.3(last accessed: 15 Dec 2016)".

4 Litchfield NJ, Benson A, Bischoff A, Hatem A, Barrier A, Nicol A, Wandres A, Lukovic B, Hall B, Gasston C, Asher C, Grimshaw C, Madugo C, Fenton C, Hale D, Barrell D, Heron D, Strong D, Townsend D, Nobe D, Howarth J, Pettinga J, Kearse J, Williams J, Manousakis J, Mountjoy J, Rowland J, Clark K, Pedley K, Sauer K, Berryman K, Hemphill-Haley M, Stirling M, Villeneuve M, Cockroft M, Khajavi N, Barnes P, Villamor P, Carne R, Langridge R, Zinke R, Van Dissen R, McColl S, Cox S, Lawson S, Little T, Stahl T, Cochran U, Toy V, Ries W, and Juniper Z (2016). "14th November 2016 M7.8 Kaikoura Earthquake. Preliminary surface fault displacement measurements. Version 2. GNS Science. http://dx.doi.org/10.21420/G2J01F ".

5 Petley DN (2016). "A revised landslide map for the M=7.8 Kaikoura earthquake: http://blogs.agu.org/landslideblog/2016/11/28/m7-8-kaikoura-earthquake/ (last accessed: 15 Dec 2016)".

6 NZTA (2016). "Kaikoura earthquake update - 20 December http://www.nzta.govt.nz/assets/traffic/Kaikoura-Earthquake-Newsletter-update-20161220.pdf (last accessed: 21 Dec 2016)".

7 Stirling M, Litchfield N, Villamor P, Van Dissen R, Nicol A, Pettinga J, Barnes P, Langridge R, Little T, Barrell D, Mountjoy J, Ries W, Rowland J, Fenton C, Hamling I, Asher C, Barrier A, Benson A, Bischoff A, Borella, Carne R, Cochran U, Cockroft M, Cox S, Duke G, Fenton F, Gasston C, Grimshaw C, Hale D, Hall B, Hao K, Hatem A, Hemphill-Haley M, Heron D, Howarth J, Juniper Z, Kane T, Kearse J, Khajavi N, Lamarche G, Lawson S, Lukovic B, Madugo C, Manousakis I, McColl S, Noble D, Pedley K, Sauer K, Stahl T, Strong D, Townsend D, Toy V, Villeneuve M, Wandres A, Williams J, Woelz S, and Zinke R (2017). "The Mw7.8 2016 Kaikura earthquake: Surface fault rupture and seismic hazard context". *Bulletin of the New Zealand Society for Earthquake Engineering*, **50**(2): 73–84.

8 Hamling I (2016). "Preliminary source inversion of the 14 November 2016 Mw7.8 Kaikoura earthquake (personal communication)".

9 Bradley BA, Razafindrakoto HNT, and Polak V (2017). "GroundMotion Observations from the 14 November 2016 Mw7.8 Kaikoura, New Zealand, Earthquake and Insights from Broadband Simulations". *Seismological Research Letters*, **88**(3): 740–756, DOI: 10.1785/0220160225.

10 NIWA (2016). ""Scientists detect huge fault rupture offshore from Kaikoura" https://www.niwa.co.nz/news/scientists-detect-huge-fault-rupture-offshore-from-kaikoura 22 November 2016 (last accessed 20 Dec 2016)".

11 Stirling M, McVerry G, Gerstenberger M, Litchfield N, Van Dissen R, Berryman K, Barnes P, Wallace L, Villamor P, Langridge R, Lamarche G, Nodder S, Reyners M, Bradley B, Rhoades D, Smith W, Nicol A, Pettinga J, Clark K, and Jacobs K (2012). "National seismic hazard model for New Zealand: 2010 update". *Bulletin of the Seismological Society of America*, **102**(4): 1514–1542, DOI: 10.1785/0120110170, URL: http://www.bssaonline.org/content/102/4/1514.abstract.

12 Van Houtte C, Bannister S, Holden C, Bourguignon S, and McVerry G (2017). "The New Zealand Strong Motion Database". *Bulletin of the New Zealand Society for Earthquake Engineering*, **50**(1): 1–20.

13 Bradley BA and Cubrinovski M (2011). "Near-source Strong Ground Motions Observed in the 22 February 2011 Christchurch Earthquake". *Seismological Research Letters*, **82**(6): 853–865, DOI: 10.1785/gssrl.82.6.853, URL: http://srl.geoscienceworld.org.

14 Fry B, Benites R, and Kaiser A (2011). "The Character of Accelerations in the Mw 6.2 Christchurch Earthquake". *Seismological Research Letters*, **82**(6): 846–852, DOI: 10.1785/gssrl.82.6.846, URL: http://srl.geoscienceworld.org.

15 Aoi S, Kunugi T, and Fujiwara H (2008). "Trampoline Effect in Extreme Ground Motion". *Science*, **322**(5902): 727–730, DOI: 10.1126/science.1163113, URL: http://www.sciencemag.org/content/322/5902/727.abstract.

16 Yamada M, Mori J, and Heaton T (2009). "The Slapdown Phase in High-acceleration Records of Large Earthquakes". *Seismological Research Letters*, **80**(4): 559–564, DOI: 10.1785/gssrl.80.4.559, URL: http://srl.geoscienceworld.org.

17 Tobita T, Iai S, and Iwata T (2010). "Numerical Analysis of Near-Field Asymmetric Vertical Motion". *Bulletin of the Seismological Society of America*, **100**(4): 1456–1469,

DOI: 10.1785/0120090301, URL: http://www.bssaonline.org/content/100/4/1456.abstract.

18 Jeong S and Bradley BA (2016). "Simulation of strong asymmetrical vertical acceleration at Heathcote Valley in the 2010-2011 Cantebury earthquakes". *New Zealand Society for Earthquake Engineering Annual Conference*.

19 NZS11705 (2004). "Structural design actions, Part 5: Earthquake actions - New Zealand": 82.

20 Kaiser A, Van Houtte C, Perrin N, Wotherspoon L, and McVerry G (2017). "Site characterisation of GeoNet stations for the New Zealand strong motion database". *Bulletin of the New Zealand Society for Earthquake Engineering*, **50**(1): 39–49.

21 Bradley B, Wotherspoon L, and Kaiser A (2017). "Ground motion and site effect observations in the Wellington region from the 2016 Mw7.8 Kaikoura, New Zealand earthquake". *Bulletin of the New Zealand Society for Earthquake Engineering*, **50**(2): 94–105.

22 Eberhart-Phillips D, Reyners M, Bannister S, Chadwick M, and Ellis S (2010). "Establishing a Versatile 3-D Seismic Velocity Model for New Zealand". *Seismological Research Letters*, **81**(6): 992–1000, DOI: 10.1785/gssrl.81.6.992, URL: http://srl.geoscienceworld.org.

23 Lee R, Bradley B, Ghisetti F, and Thomson E (2016). "Development of a 3D high-resolution velocity model for the Canterbury, New Zealand region". *Bulletin of the Seismological Society of America (submitted)*.

24 Worden CB, Gerstenberger MC, Rhoades DA, and Wald DJ (2012). "Probabilistic Relationships between Ground-Motion Parameters and Modified Mercalli Intensity in California". *Bulletin of the Seismological Society of America*, **102**(1): 204–221, DOI: 10.1785/0120110156, URL: http://www.bssaonline.org/content/102/1/204.abstract.

25 Bradley BA (2013). "A New Zealand-Specific Pseudospectral Acceleration Ground-Motion Prediction Equation for Active Shallow Crustal Earthquakes Based on Foreign Models". *Bulletin of the Seismological Society of America*, **103**(3): 1801–1822, DOI: 10.1785/0120120021, URL: http://www.bssaonline.org/content/103/3/1801.abstract.

26 Afshari K and Stewart JP (2016). "Physically Parameterized Prediction Equations for Significant Duration in Active Crustal Regions". *Earthquake Spectra*, **32**(4): 2057–2081, DOI: 10.1193/063015eqs106m, URL: http://earthquakespectra.org/doi/abs/10.1193/063015EQS106M.